ELECTROLUMINISCENCE IMAGING AND LIGHT BEAM INDUCED CURRENT AS CHARACTERIZATION TECHNIQUES OF MULTI-CRYSTALLINE SI SOLAR CELLS

L.A. Sánchez, A. Moretón, M. Jiménez, M. Guada, S. Rodríguez-Conde, M. A. González, O. Martínez and J. Jiménez
GdS-Optronlab, Dpto. Física de la Materia Condensada
Universidad de Valladolid, Edificio LUCIA, Paseo de Belén 19, 47011 Valladolid, Spain.

ABSTRACT: There is an increasing demand for characterizing multicrystalline solar cells at different stages of its service life. Luminescence techniques, e.g. electroluminescence (EL) and photoluminescence (PL), have acquired a paramount interest in the last years. These techniques are used in imaging mode, allowing to take a luminescence picture at a full wafer/cell scale. This imaging approach is fast and sensitive, but has a low spatial resolution, which avoids a detailed analysis of the defect distribution, which can led to misinterpretations about critical parameters as the minority carrier diffusion length, or the internal and external quantum efficiencies. If one complements these techniques with high spatial resolution techniques, such as light beam induced current (LBIC), one can study the electrical activity of the defects at a micrometric scale, providing additional understanding about the role played by the defects in full wafer/cell luminescence images. The combination of the macroscopic and microscopic resolution scales is necessary for the analysis of the full luminescence images in mc-Si solar cells.
KEYWORDS: Solar cells, multicrystalline silicon, UMG silicon, LBIC, photoluminescence.

1. INTRODUCTION:

Photovoltaic (PV) industry is currently dominated by multicrystaline silicon (mc-Si), due its cost-efficiency ratio. The traditional purification method of metalurgical grade silicon is called Siemens process [1]. This process permits to obtain high-quality solar-grade Silicon (SoG-Si), but it is a very energy-intensive process. SoG-Si produced through metallurgical purification processes is called upgraded metallurgical-grade silicon (UMG Si), and it appears as an alternative method to the Siemens procedure due to its reduced production cost and time [2].

Characterization of the electrical activity in UMG Si solar cells is essential to know the distribution of impurities and how they interact with the crystal defects, namely grain boundaries, and intragrain defects, and thereafter how they can affect the cell efficiency [3]. Luminiscence imaging, both electroluminescence (ELi) and photoluminescence (PLi), and light-beam induced current (LBIC) are powerful techniques for the study of the electrical activity of those defects, and the quantum efficiency (QE) [4-7].

ELi is captured on a forward biased solar cell, while PLi is excited by an homogeneously dispersed laser beam. These techniques can provide a full image of the solar cell in a few milliseconds, which promises its in line use. The EL intensity signal is proportional to the excess minority carrier density, so áreas with a high non radiative recombination centers (NRRCs) density appear as dark contrasted. These regions are usually associated with dislocations, grain boundaries (GBs), micro cracks or defective contacts, also impurities can play a relevant role, especially in poorly purified feddstock. In order to relate Eli/Pli images to the cell efficiency the characterization of the contrast in the ELi/PLi must be done .

In LBIC technique, a laser beam is focused on the cell surface using an optical microscope and it is scanned over a surface area of the cell. The photogenerated carriers produce a current which the intensity depends on the trapping of minority carriers. At least two laser wavelengths are necessary to obtain the quantum efficiency of the explored areas of the cell. This technique permits to record high spatial resolution maps (up to 1 µm) at the expense of long acquisition times. We compare herein the results obtained by Eli/PLi and LBIC on UMG-Si solar cells.

2. EXPERIMENTAL:

UMG mc-Si solar cells were characterized by the ELi /PLi and LBIC techniques. The measurements were carried out on a series of UMG mc-Si solar cells with efficiencies varying between 15 and 18.4%.

A homemade LBIC system was used to obtain detailed information about the defects in the solar cells [8]. The scheme of the LBIC setup is shown in Fig. 1. The LBIC apparatus consists of two dual laser diodes providing four excitation wavelengths (639, 830, 853 and 975 nm), allowing different penetration depths in the cell. In this study the 853 nm and 975 nm lines were used. A beam-splitter divides the output beam of the laser (10 mW) into two beams. One of them is used to measure variations of the output power through a photodiode, while the other one is directed into a trinocular microscope, which focuses the laser beam onto the solar cell. Different objectives (20x, 50x, 100x) enable studies at different spatial resolutions, up to 1 µm using the 100x objective, 0,95 numerical aperture (NA). A Si-CCD camera coupled to the microscope ocular is used to collect the light reflected by the sample to drive the auto-focus system. The LBIC scanning is done by moving the sample with a high precision *x-y-z* motorized translation stage (Prior Scientific) over areas as large as 76.7 x 114.5 mm^2 and step sizes as small as 1 µm. The photocurrent is measured by an electrometer (Keithley Instruments). Data acquisition and hardware control were developed in LabVIEW.

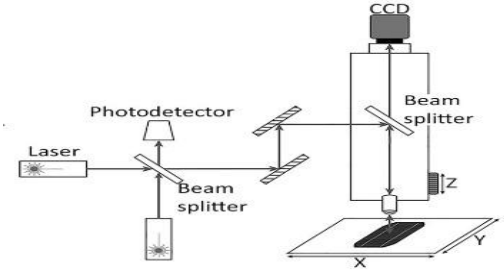

Fig. 1. Scheme of the LBIC system

The Eli/PLi images were acquired using a homemade dual system. A high power 808 nm laser diode was used as the excitation source for PLi measurements. Both PL and El images were acquired with an InGaAs camera.

3. RESULTS AND DISCUSSION:

Figures 2a-c show the EL images obtained in three solar cells, labelled A, B and C, corresponding to different efficiency series, table I. These cells correspond to wafers cut on different positions of the same brick. One can distinguish some patterns common to the three cells, corresponding to grains extending along the brick because of the columnar growth along the solidification direction [9].

The ELi contrast differs for the three cells depending on the position of the wafers in the brick, due to the impurity incorporation gradient, consequence of the directional solidification. At a glance one can establish a correlation between the cell efficiencies, table I, and the darkness of the EL images.

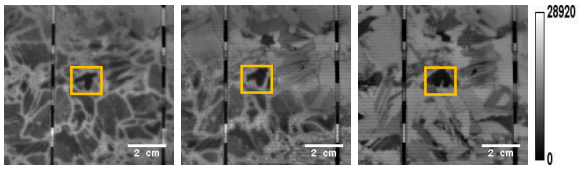

Fig. 2. (a—c) EL images of three solar cells with different efficiencies. The marked areas indicate the zones where LBIC measurements were carried out.

Surprisingly, the grain boundaries (GBs) and intragrain defects in cells A and B present bright contrast, while inside the grains a dark contrast is observed. In order to rule out the possible contribution to this contrast of leakage currents across the GBs [10], photoluminescence images (PLi) were also acquired. The PLi results were similar to ELi; therefore, the bright contrast of the grain boundaries and defects cannot be associated with leakage currents, but with the impurity distribution, and its interaction with the crystal defects. Due to the directional solidification process impurities accumulate in a higher concentration in the upper part of the ingot [9].

The EL intensity calculated as the sum over all the image pixels for the EL image shows a good correlation with the cell efficiency, [11]. A nearly linear correlation between the EL intensity and the cell efficiency was appreciated; evidencing that Eli can be a powerful tool for estimating the cell efficiency

	A	B	C	D
Power (W)	3.85	4.19	4.31	4.46
Average Efficiency(%)	15-16.6	17.2-17.4	17.7-17.8	18.3-18.4

Table. I. Cell efficiencies. A, B and C wafers come from the same mc-Si brick. A is from the top of the brick, B is close to A, and C is closer to the middle of the brick. D is from a different brick.

The LBIC measurements were carried out over the square regions indicated in Figures 1a—c with a 20x objective. 1.8 x 1.8 cm^2 short-circuit current maps obtained with the 853 nm laser are shown in Figures 3a—c. The spatial resolution obtained with the LBIC system allows a more detailed study of the GBs and intragrain defects. In figures 3a and 3b one observes the dark contrast for these defects surrounded by a bright contrasted halo.

Instead of the bright contrast observed in the Eli/PLi images; this discrepancy is due to the different spatial resolutions. The narrow dark contrast lines along the GBs and intragrain defects revealed by LBIC cannot be observed at the full cell scale resolution of the Eli/PLi measurements. The LBIC signal distribution is the consequence of the gettering of impurities by the grain boundaries and the intragrain defects, which leave the surrounding areas depleted of impurities. The impurities are gettered by the strain field of the grain boundaries and dislocations during the solidification. The C series solar cells (figure 3c) do not present this effect and the GBs loss the electrical activity observed in the cells of the upper part of the brick. Note that the GB activity is more marked for cells of type A in which the concentration of impurities is significantly higher as seen by the dark grain bodies as compared to cells B and especially cells C, where the grain cores give bright contrast. This suggests that the electrical activity of the GBs is mainly related to the capture of impurities, and therefore it is governed by the feestock purity[11,12].

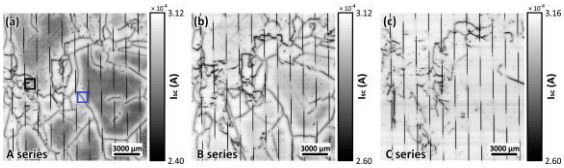

Fig. 4. (a—c) LBIC maps of the square regions indicated in Fig. 2a—c, obtained with an 853 nm laser (1.8 x 1.8 cm2, 20x objective, step size 90 µm).

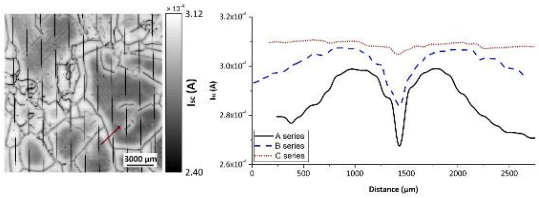

Fig. 5. a) LBIC map of the square region corresponding to A-series solar cell b) LBIC intensity profiles along the red arrow in the LBIC image for A, B and C solar cells series

LBIC intensity profiles across a GB are shown in Fig. 5 for the three cells, A, B and C. A profound carrier depletion is observed for cell A, the depletion is reduced for cell B, and is almost negligible for cell C. This points to the importance of the impurities in the electrical activity of the GBs, the higher the impurity concentration the higher the GB electrical activity. As revealed by the LBIC images, the GBs getter the impurities around them, and the dark contrast at the GBs seems to be related to the presence of impurities, reducing its carrier trapping activity as the material putity improves.

On the other hand, the presence of defects and impurities determines the minority carrier diffusion length (L_{eff}), which can be estimated from the internal quantum efficiencis (IQE) obtained from the LBIC maps for two excitation wavelengths (853 and 975 nm), according to the expression [13]:

$$\frac{1}{IQE(\lambda)} \approx 1 + \frac{1}{\alpha(\lambda) L_{eff}}$$

where $\alpha(\lambda)$ is the Si absorption coefficient at 300 K (534 cm^{-1} for 853 nm and 106 cm^{-1} for 975 nm).
The calculated diffusion length maps for samples A, B and C are shown in Fig. 6

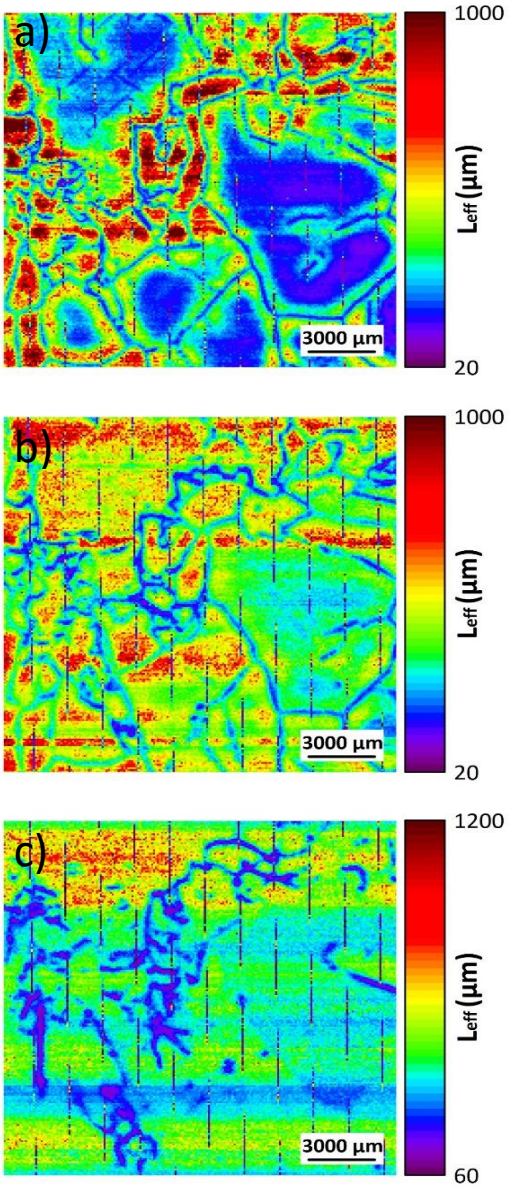

Fig. 6. L_{eff} maps of the A, B and C-series solar cell obtained with 853 nm and 975 nm lasers

The diffusion length increases from A to C. In sample A the diffusion length is severely reduced inside the grains, while it increases around the defects because of the impurity depletion around them. This is the opposite to sample C, where the diffusion length is higher inside the grains, and appears limited at the intragrain defects formed by clusters of dislocations [14]

High resolution LBIC measurements were carried out using a 100x objective with 0.95 numerical aperture (NA). Figure 7 shows 600 x 600 µm^2 LBIC maps. In this high resolution maps one observes tiny dark spots around the defects. These tiny spots can be associated with metallic clusters without optical and electrical activity, as deduced from the absence of any contrast gradient around them. These tiny precipitates are characteristic of feedstock with low purification as UMG Si. These defects were mainly observed around intragrain defects, and much less frequently around the GBs. This behavior suggests that intragrain defects have a higher impurity gettering efficiency with respect to the GBs.

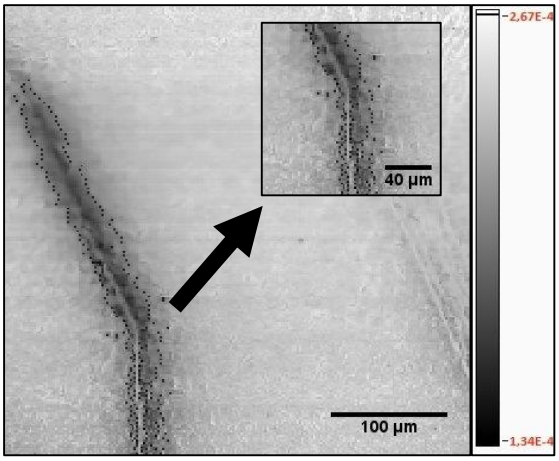

Fig. 7. High resolution LBIC map obtained with an excitation wavelength of 853 nm (600x600 µm2, 100x objective, step size 3 µm) showing an intragrain defect decorated with tiny dark spots

Figure 8 a, b and c shows 400 x 400 μm^2 LBIC maps of A, B and C-series solar cells using a 100x objective. These measurements revealed a slightly bright contrasted line along the core of the defects in all the series. This local bright contrast is due to variations in the light reflectivity.

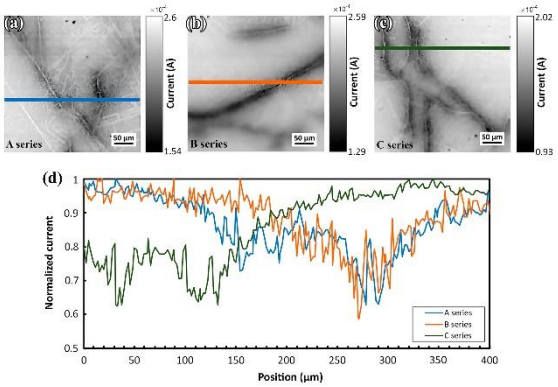

Fig. 8. (a—c) LBIC maps of defective areas in three solar cells of A, B and C series (400x400 µm^2, 100x objective, step size 2 µm). (d) Normalized photocurrent profiles across the lines marked in Fig. 8a—c.

Figure 8d shows the LBIC contrast profiles across the lines marked in Fig. 8a, b and c. This LBIC contrast is defined by

$$C = \frac{(I_b - I_d)}{I_d}$$

Where I_b is the background photocurrent measured in a defect-free region and I_d is the photocurrent measured in

a defective region. I_b (C)>I_b(B)>I_b(A), however, the contrast is similar for the three solar cells near the defects, therefore, the lower efficiencies in the A and B cells is greatly contributed by the presence of impurities inside the grains, which is significantly reduced in cell C.

4. CONCLUSIONS:

UMG Si solar cells with different efficiencies have been characterized through Eli/PLi and LBIC techniques. A full wafer study of the cells with ELi did not reveal the electrical activity of the GBs, but they were blurred by the impurity depleted area around them. High spatial resolution LBIC maps revealed the true trapping activity of the GBs. The LBIC maps of the UMG-Si cells permits to establish the influence of the impurities on the basic parameters of the cells, e.g.L_{eff}, and QE, both external and internal. Also, the interaction between crystal defects in multicrystalline Si and impurities can be analysed. The interpretation of the Eli/PLi full wafer/cell images must be complemented with high spatial resolution measurements.

5. ACKNOWLEDGEMENTS:

This work was supported by the Spanish MINECO project, ref. ENE2014-56069-C4-4-R and "Junta de Castilla y León (Spain)" project number VA081U16. We wish to thank Silicio Ferrosolar for providing the samples studied in this work.

6. REFERENCES:

1. J.O. Odden, H. Halvorsen, H. Rong and R. Gløckner in Silicon for the Chemical and Solar Industry IX (Oslo, Norway, 2008) pp. 75-90.
2. J. Safarian, G. Tranell and M. Tangstad, Energy Procedia **20**, 88-97 (2012).
3. F. Rougieux, C. Samundsett, K.C. Fong, A. Fell, P. Zheng, D. Macdonald, J. Degoulange, R. Einhaus and M. Forster; Progr. Photovolt. Res. Appl. **24**, 725-734 (2016).
4. T. Kirchartz, A. Helbig , W. Reetz , et al.; Progr. Photovolt. Res. Appl. **17**, .394-402 (2009).
5. T. Potthoff, K. Bothe, U. Eitner, et al.; Progr. Photovolt. Res. Appl. **18**, 100-106 (2010)
6. U. Rau; Phys. Rev. B, **76**, 085303 (2007)
7. T. Trupke, B. Mitchell, J. W. Weber, W. McMillan, R. A. Bardos and R. Kroeze, Energy Procedia **15**, 135-146 (2012).
8. B. Moralejo, M. A. González, J. Jiménez, V. Parra, O. Martínez, J. Gutiérrez and O. Charro, J. Electron. Mater. **39**, 663–670 (2010).
9. T. Liu, Z. Dong, Y. Zhao, J. Wang, T. Chen, H. Xie, J. Li, H. Ni and D. Huo, J. Cryst. Growth **355**, 145-150 (2012)
10. O. Breitenstein, J.P. Rakotoniaina, M.H. Al Rifai, M. Werner; Progr. Photovolt. Res. Appl. **12**, 529-538 (2004)
11. L.A.Sánchez, A. Moretón, M. Guada, S. Rodríguez-Conde, O. Martínez, J. Jiménez; MRS Advances 2018 DOI: 10.1557/adv.2018.366
12. T. Buonassisi et al.; Progr. Photovolt. Res. Appl **14**, 513-531 (2006)
13. M.K. Juhl, M.D. Abbott, T. Trupke, IEEE J. Photovolt. **7**, 1074–1080 (2017).
14. B.R. Ryningen, G. Stokkan, M. Kivambe, T.Ervik, O. lohne; Acta Mater. **59**, 7703-7710 (2011)